Electronic Supplementary Information

Electrochemical deposition and thermoelectric characterisation of a semiconducting 2-D metal-organic framework thin film.

Maria de Lourdes Gonzalez-Juarez[a], Eduardo Flores[b], Marisol Martin-Gonzalez[b], Iris Nandhakumar[a], Darren Bradshaw*[a]*

[a]School of Chemistry, University of Southampton, Southampton SO17 1BJ, UK

Email: D. Bradshaw@soton.ac.uk; I.Nandhakumar@soton.ac.uk

[b]Instituto de Micro y Nanotecnología (CNM-CSIC), C/ Isaac Newton 8, PTM, E-28760 Tres Cantos, Spain

Experimental methods

Materials

Copper(II) nitrate trihydrate, copper(II) sulfate pentahydrate (ACS reagent, ≥98.0%), potassium chloride (ACS reagent, 99.0 %), poly(methyl methacrylate) (MW ~120,000), chlorobenzene (99.8%), ethanol absolute, and ammonium hydroxide solution (ACS reagent, 28.0-30.0% NH_3 basis) were purchased from Sigma-Aldrich. 2,3,6,7,10,11-hexahydroxytriphenylene hydrate (HHTP, ≥95%) was purchased from TCI Europe. Tributylmethylammonium methyl sulfate (MTBS) was purchased from Santa Cruz. All reagents and solvents were used as received without further purification. Ultrapure Milli-Q water with a resistivity higher than 18 MΩ·cm was used to prepare the solutions. Au coated silicon and fluorine-tin oxide glass (FTO, 15 Ω) were used as working electrodes.

Characterisations

The crystal structure of $Cu_3(HHTP)_2$ in bulk was determined by Powder X-ray diffraction (PXRD) using a Bruker D2 phaser diffractometer, CuKα radiation, λ=1.5406 Å. The MOF powder was placed on a zero background Si holder. In order to determine the lattice parameters Rietveld refinement was conducted by using GSAS-II software. The experimental PXRD pattern was refined to an AA packing mode assuming a P6/mmm hexagonal symmetry. Refining in this space group lowers the deviation to unrealistic lattice parameters values by reducing the number of refined parameters and locking the gamma angle at 120°. Contrary to what would happen if a P1 symmetry was assumed, since there is more freedom in the model relative to the experimental data. The AB packing mode was observed to break the hexagonal symmetry because of the position of the 6-fold axis shifts in each plane. Since the difference between the AA and AB stacking arrangement is considerably small, a much higher resolution PXRD pattern is required to distinguish them. Consequently, we refined our data against the higher symmetry model.

Grazing incidence X-ray diffraction (GIXRD) was conducted using a Rigaku Smartlab, CuKα radiation, λ=1.5406 Å. Thermal gravimetric analysis (TGA) measurements were performed using a Libra Netzsch instrument under air atmosphere at a flow rate of 50 ml min^{-1} with a 10°C min^{-1} ramp. Electrical measurements were conducted using a commercial ECOPIA Hall effect measurement system. Morphological and thickness characterisations were carried out using a scanning electron microscope JEOL JSM-6500F.

Methods

Solvothermal synthesis of $Cu_3(HHTP)_2$

$Cu_3(HHTP)_2$ was synthesised hydrothermally according to the procedure reported recently by Hoppe et al.[1] To a solution of 127 mg (0.53 mmol) $Cu(NO_3)_2$ $3H_2O$ in 2 mL (111 mmol) distilled water, then 50 equivalent (270 µL) of concentrated NH_4OH was added leading to a dark blue solution. This mixture was added to a dispersion of 103 mg (0.30 mmol) of HHTP in 8.4 mL of dist. H_2O and sonicated for 10 minutes. The reaction vessel was sealed and placed in a pre-heated oven at 80 °C for 24 h. The dark precipitate was collected by centrifugation at 11,000 rpm for 15 min and washed with ethanol (5 mL x 7) and water (5 mL x 7). Yield = 60%.

Two-Step Anodic Electrosynthesis of $Cu_3(HHTP)_2$ on Transparent Conducting Substrates

Fluorine-tin oxide coated (FTO) glass (15 Ω, 10 x 20 mm) was used as working electrode. The exposed area in contact with the electrolyte was 1 cm^2. The FTO glasses were ultrasonically cleaned in 1 M HCl, isopropyl alcohol (IPA), acetone, and deionized water for 10 minutes each. Finally, the substrates were dried under an Ar stream.

Step 1. Electrodeposition of Cu@FTO

The electrolyte for the copper electrodeposition was made of a solution containing 0.01 M $Cu(SO)_4$ and 0.1 KCl as supporting electrolyte. A SCE electrode and Pt gauze were used as reference and counter electrodes, respectively. The solution was degassed with Ar for 20 minutes. A potential of -0.8 V was applied for 1 hr. The resultant deposit was rinse in H_2O and EtOH and le to dry.

Step 2. Electrodeposition of $Cu_3(HHTP)_2$@FTO

A solution containing 5 mM of the ligand HHTP and 0.02 M MTBS as supporting electrolyte in a solvent ratio 80:20 EtOH:H_2O was prepared. The working electrolyte was degassed with Ar for 10 Saturated Calomel Electrode and Pt gauze were used as reference and counter electrodes, respectively. The applied potentials were 0.435 V, 0.5 V, 0.6 V and 0.7 V for 60 min. The resultant deposit was washed with EtOH.

Transferring method of electrodeposited $Cu_3(HHTP)_2$ thin films

A suspension of poly(methyl methacrylate) (PMMA) was prepared by adding 3.71 g of PMMA in 10 mL of chlorobenzene. The suspension was stirred at 700 rpm overnight to ensure the complete dissolution of PMMA. The PMMA suspension was drop casted onto the electrodeposited $Cu_3(HHTP)_2$. Then, PMMA/$Cu_3(HHTP)_2$/Au/SiO_2 was placed on a hot plate at 40 °C overnight to form a PMMA layer. After this step, the substrate was removed from the hot plate and allowed to cool down. The PMMA/$Cu_3(HHTP)_2$ was carefully peeled off from the Au/SiO_2 substrate and characterised afterwards.

Two-Step Anodic Electrosynthesis of $Cu_3(HHTP)_2$ onto Au/SiO_2 substrates

Au/SiO_2 substrates (10 x 20 mm) were used as working electrodes. Pt gauze and SCE electrode were used as counter and reference electrodes, respectively.

The Au/SiO_2 substrates were cleaned ultrasonically in 0.1 M HCl, DI water, acetone for 15 minutes each and then dried under Ar stream.

In order to determine the reduction potential at which the Cu deposition occurs, cyclic voltammetry was conducted on Au/SiO2 electrode (exposed area ~ 1 cm^2) in a solution containing 0.01 M $CuSO_4$ and 0.1 M of KCl . The potential sweep was from -1.5 V to +1.1 V at a scan rate of 120 mV/s.

Step 1. Electrodeposition of $Cu@Au/SiO_2$

The electrolyte for the copper electrodeposition was made of a solution containing 0.01 M $CuSO_4$ and 0.1 KCl as supporting electrolyte. Saturated Calomel Electrode (SCE) and Pt gauze were used as reference and counter electrodes, respectivel**y. The solution was degassed with Ar for 10 minutes. A potential of -0.270 V was applied for 60 min.

Step 2. Electrodeposition of $Cu_3(HHTP)_2@Au/SiO_2$

A solution containing 2.5 mM of the ligand HHTP and 0.02M MTBS as supporting electrolyte in a solvent ratio 80:20 EtOH:H_2O was prepared. The working electrolyte was degassed with Ar for 10 min. Saturated Calomel Electrode and Pt gauze were used as reference and counter electrodes, respectively. The anodic dissolution of $Cu@Au/SiO_2$ was conducted at a potential of 0.435 V for 2h. Samples were characterised by GIXRD, SEM and electrical measurements.

Table S1. Summary of conductivity data for the $Cu_3(HHTP)_2$ framework reported to date.

Metal-Organic Framework	**Synthesis method**	**BET surface area (m^2 g^{-1})**	**Conductivity (S cm^{-1})**	**Morphology**	**Potential Application**	**Ref.**
$Cu_3(HHTP)_2$	Solvothermal	540	N.R.	nanowires	Solid-state capacitors	1
" "	Solvothermal	N.R.	~0.2 (single crystal; 4-point)	hexagonal rods	Energy storage	2
" "	Solvothermal	N.R.	0.002 (pellet; 2-probe)	irregular shape	Chemiresistive sensors	3
" "	Mother solution	N.R.	N.R.	nanorods	Chemiresistive sensors	4
" "	Solvothermal	78	N.R.	needles	Catalysis	5
" "	Layer-by-Layer	N.R.	0.02 (film; 2-probe)	irregular shape	Chemiresistive sensors	6
" "	Liquid-liquid interface	N.R.	10^{-4} (film, N.R.)	nanosheets	Field-effect transistors	7
" "	Solvothermal	512	0.045 (pellet; van der Pauw)	flake-like particles	N.A.	8
" "	Spray-coating	N.R.	0.023 (film; van der Pauw)	flake-like particles	MeOH sensing	8
" "	Hydrothermal	284	0.02 (pellet, 4-point)	nanorods	Chemiresistive sensors	9
" "	Layer-by-Layer	N.R.	0.03 (film, 2-probe)	layers	Organic spin valves	10
" "	Solvothermal	340.5	N.R.	nanowires	Capacitors	11
" "	Solvothermal	154	0.02 (film)	nanowires	anode Li-batteries	12
" "	Solvothermal	151.95	N.R.	nanoparticles	Chemiresistive sensors	13
" "	Solvothermal	N.R.	0.01 (bulk, 2-probe)	nanorods	Cathode Zn-batteries	14
" "	Solvothermal	506.08	N.R.	nanosheets	Cathode Li-batteries	15
" "	Solvothermal	306	0.027 (pellet, Van der Pauw)	needles	Energy	16

Table S2. Thermoelectric properties of MOFs reported to date.

Metal-Organic Framework	**Synthesis method**	**Thermal Conductivity (W m^{-1} K^{-1})**	**Conductivity (S cm^{-1})**	**Seebeck coefficient (µV K^{-1})**	**Power Factor (µW m^{-1} K^{-2})**	**Figure of merit**	**Ref.**
TCNQ@HKUST-1	Liquid-phase (film)	0.27	~4 x 10^{-3}	375 (@298 K)	0.057	7 x10^{-5}	17
TCNQ@HKUST-1	Liquid-phase (film)	N.R.	~3 x10^{-3}	342.39 (@290 K)	0.035	-	18
$Ni_3(HITP)_2$	Solvothermal (pellet)	0.21	58.8	-11.9 (@298 K)	0.831	1.19 x10^{-3}	19

Additional figures

Fig S1. Statistics and figures of merit of different types of thermoelectric materials surveyed by 2019. Adapted from reference 20.

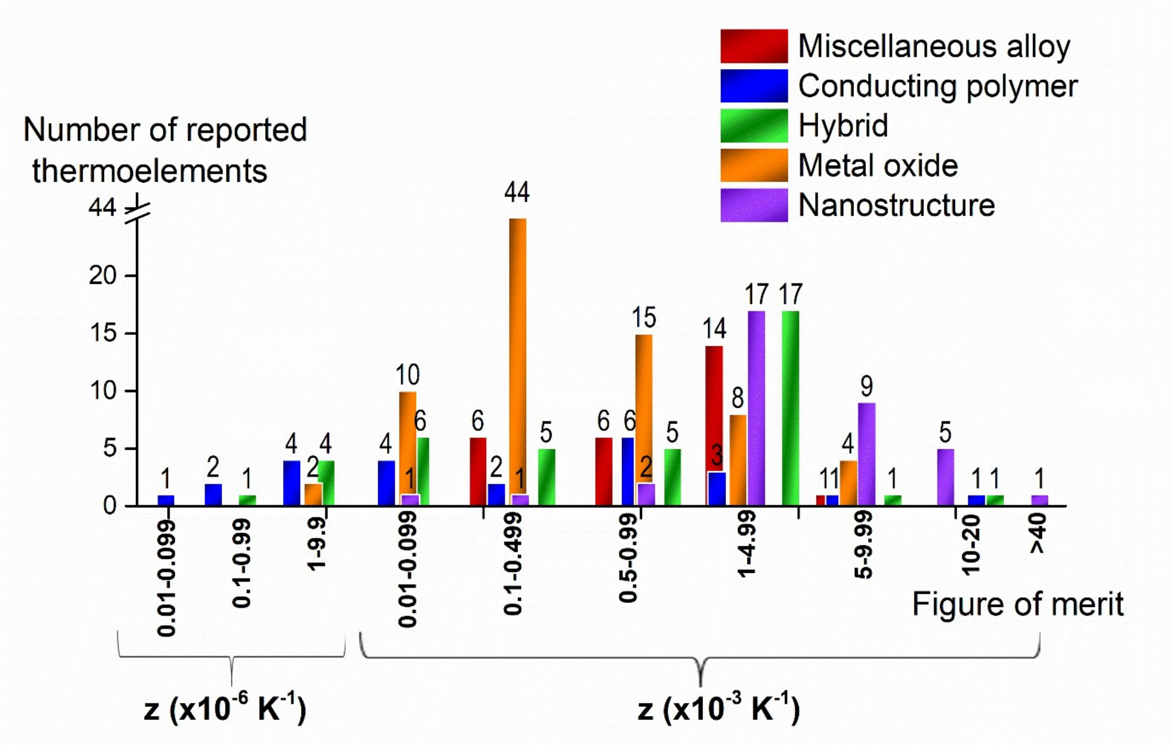

Figure S2. Structural representations of the $Cu_3(HTTP)_2$ framework refined from bulk powder data in an AA stacking motif. Copper (orange), carbon (grey) and oxygen (red).

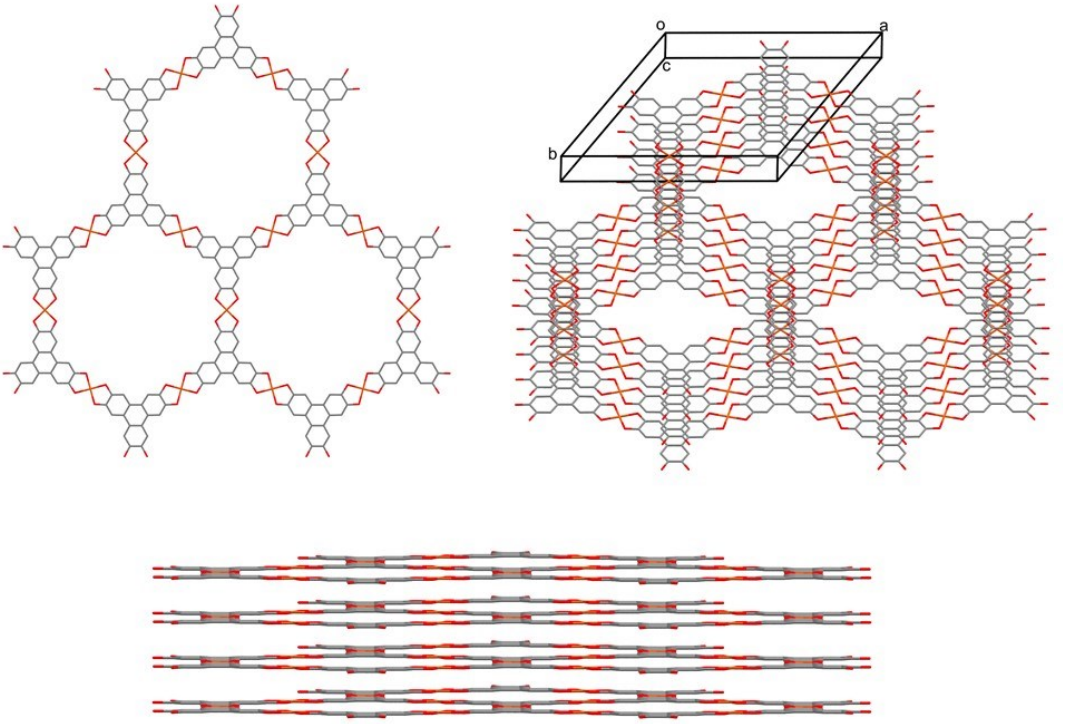

Figure S3. SEM images of $Cu_3(HHTP)_2$ powder synthesised hydrothermally.

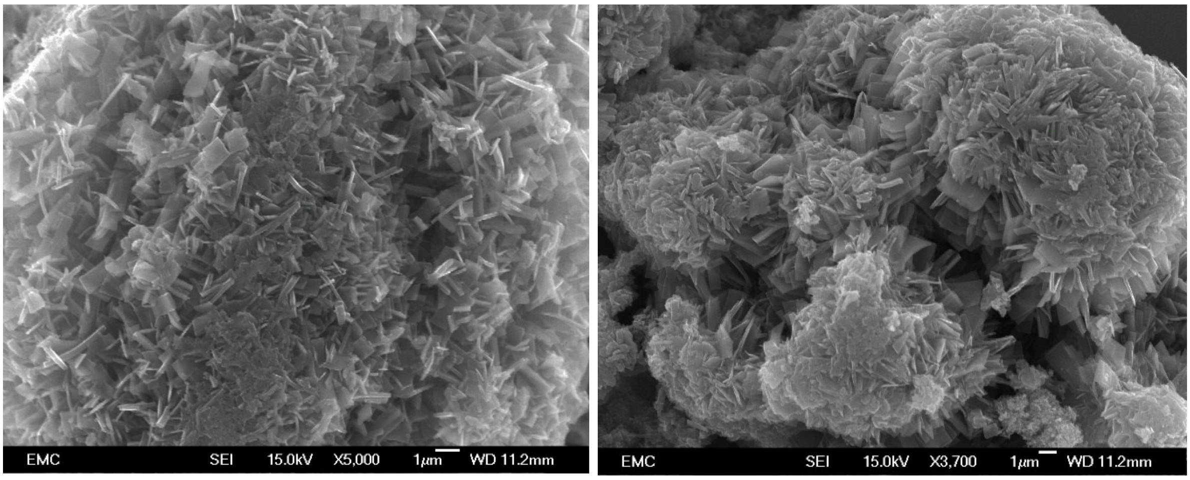

Figure S4. SEM cross section images of the $Cu_3(HHTP)_2$ pellet formed from the bulk powder sample shown in figure S1.

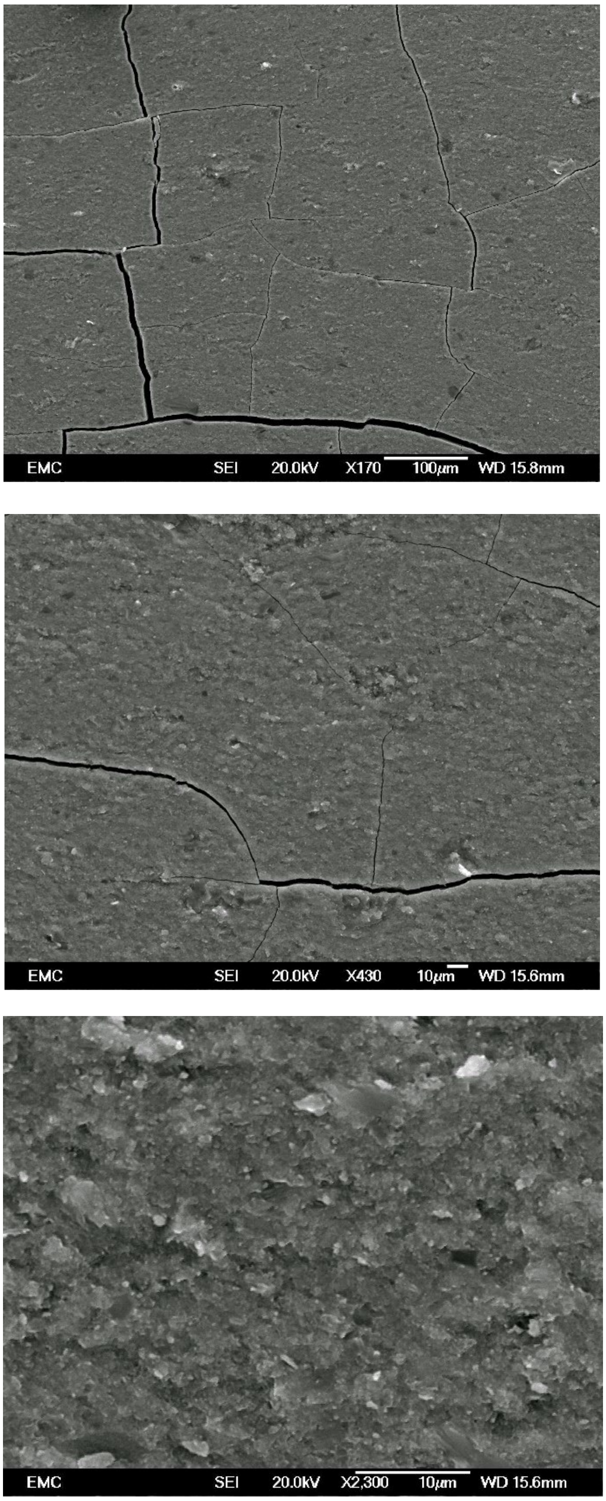

Figure S5. Home-built Seebeck apparatus used for thermopower measurements.

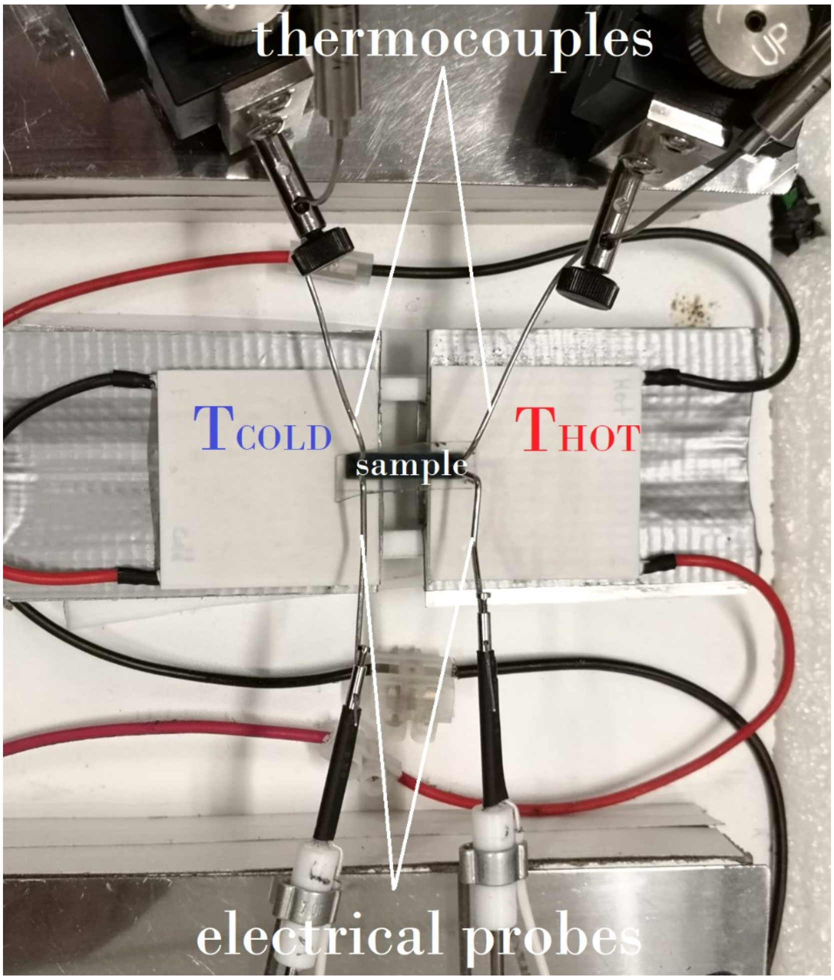

Figure S6. I-V curves of $Cu_3(HHTP)_2$ configured as a pellet (left) and the electrodeposited thin film (right) A, B, C and D are assigned to each one of the four probes placed on the sample. The AB curve corresponds the electrical response recorded from probe A to probe B and so on. The gradient of the slope in the I-V curves is correlated to the geometry and distance between the electrical probes. For instance, the more the separation between the probes, the higher the resistivity is due to a larger electron scattering, therefore, the voltage response is lower in accordance to Ohm's law.

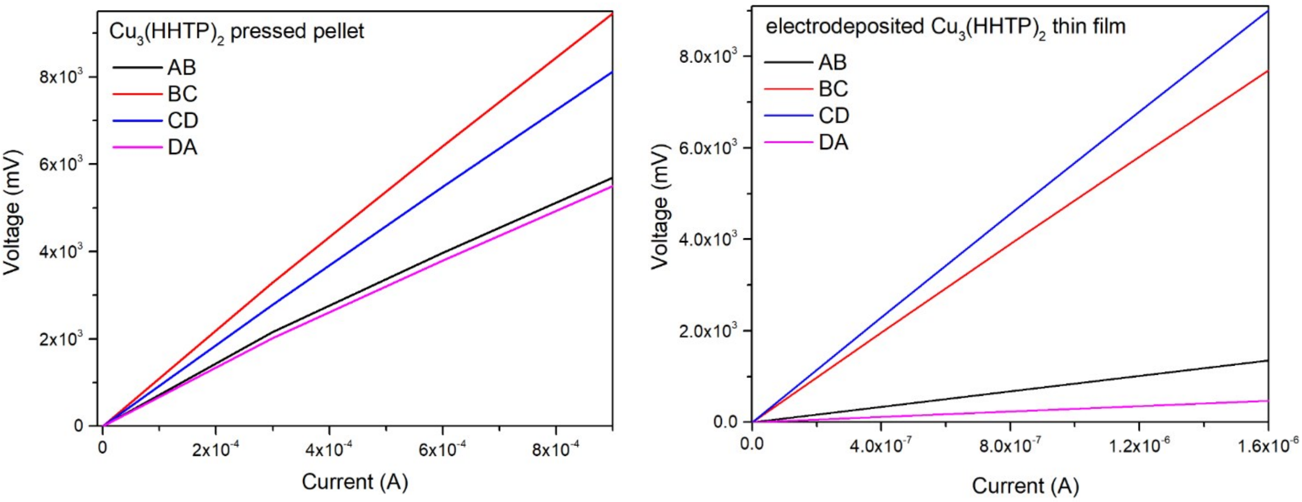

Table S3. GXRD data of electrodeposited $Cu_3(HHTP)_2$ thin films on FTO.

	Applied potential (V)							
	0.435		**0.5**		**0.6**		**0.7**	
Crystal plane	**Peak position**	**FWHM**	**Peak position**	**FWHM**	**Peak position**	**FWHM**	**Peak position**	**FWHM**
200	9.65	0.5788	9.54	0.5628	9.63	0.4557	9.6	0.7996
210	12.72	0.469	12.77	0.8375	12.59	1.1314	12.72	1.0797
220	28.08	1.6103	27.81	1.7813	27.96	1.8502	28.07	1.669

*Full width at half maximum (FWHM)

Figure S7. Arrhenius plots of $Cu_3(HHTP)_2$ pellet (left) and thin film (right) for the determination of the band gap. The natural logarithm of the electrical conductivity (σ) data is plotted as a function of 1/T. Data comprises three σ readings per temperature set point as shown in the graphs. The activation energy is then obtained from the resultant slope of the linear fit, being 2.68 eV and 2.61 eV for the pellet and film, respectively. These band gaps are large enough to ensure that no photo-thermolectric responses are likely to be observed using the set-up shown in figure S5.

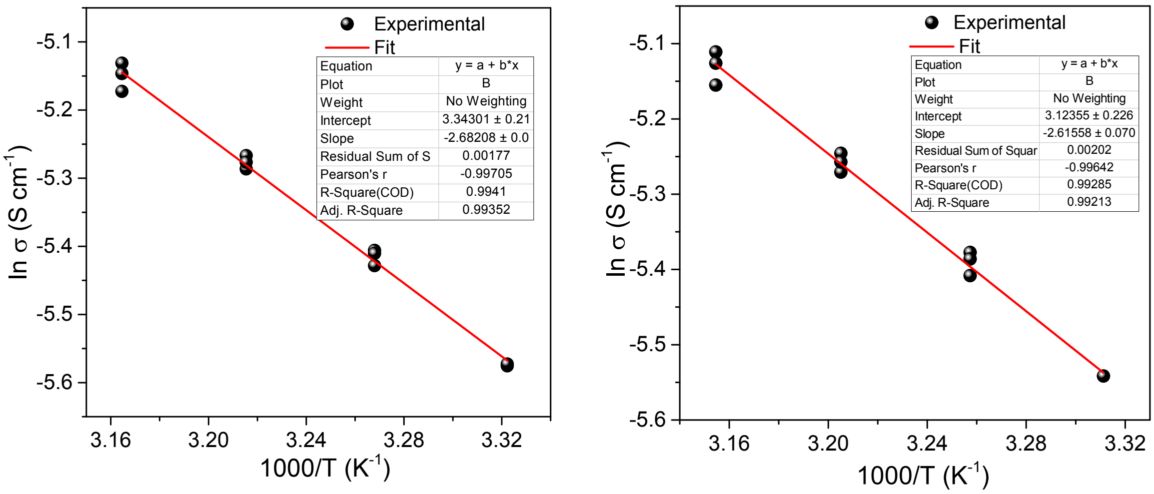

Equation	y = a + b*x
Plot	B
Weight	No Weighting
Intercept	3.34301 ± 0.21
Slope	-2.68208 ± 0.0
Residual Sum of S	0.00177
Pearson's r	-0.99705
R-Square(COD)	0.9941
Adj. R-Square	0.99352

Equation	y = a + b*x
Plot	B
Weight	No Weighting
Intercept	3.12355 ± 0.226
Slope	-2.61558 ± 0.070
Residual Sum of Squar	0.00202
Pearson's r	-0.99642
R-Square(COD)	0.99285
Adj. R-Square	0.99213

Figure S8. Cross section SEM images of a) the electrodeposited copper film on FTO glass and b) the subsequent $Cu_3(HHTP)_2$ film synthesised electrochemically. c) GIXRD pattern of electrodeposited Cu on FTO glass.

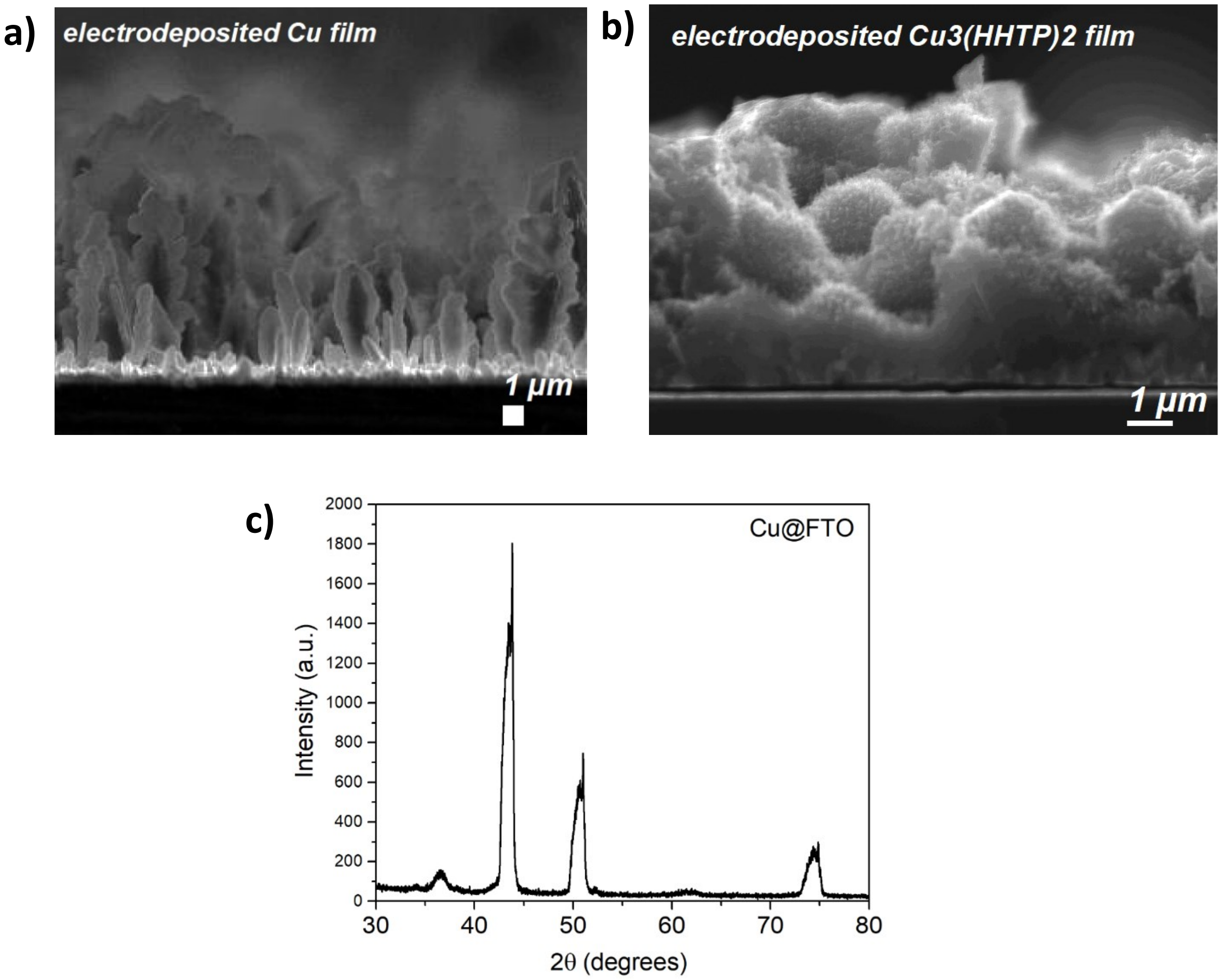

Figure S9. Voltammogram of Au/SiO_2 electrode in 0.01 M $CuSO_4$ and 0.1 M KCl as supporting electrolyte. Scan rate 120 mV s^{-1}. Electrode area: 1 cm^2. Potential swept from -1.1 V to +0.9 V.

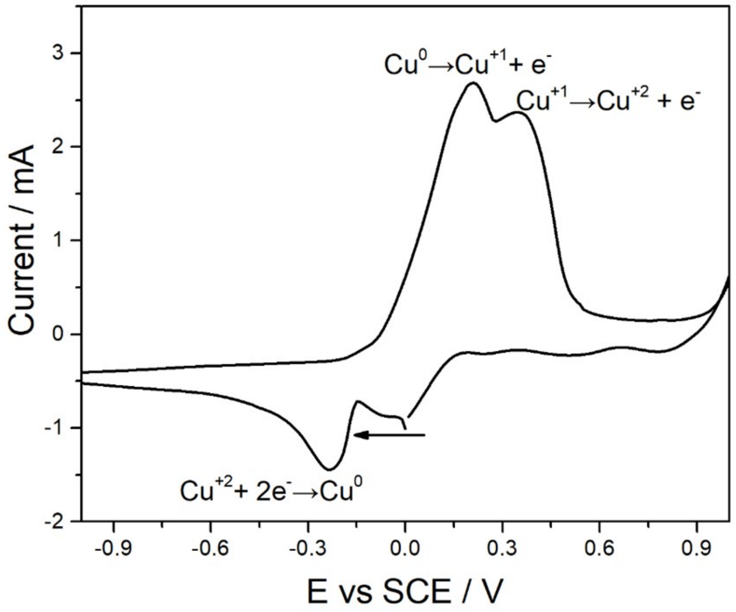

Figure S10. SEM top view image of the PMMA transferred $Cu_3(HHTP)_2$ film synthesised electrochemically (top). For cross-sectional imaging, $Cu_3(HHTP)_2$ thin films were transferred using a commercial 2-part epoxy adhesive instead of PMMA. The transfer procedure is the same as stated in the methods section, with the exception that the PMMA is replaced by the epoxy.

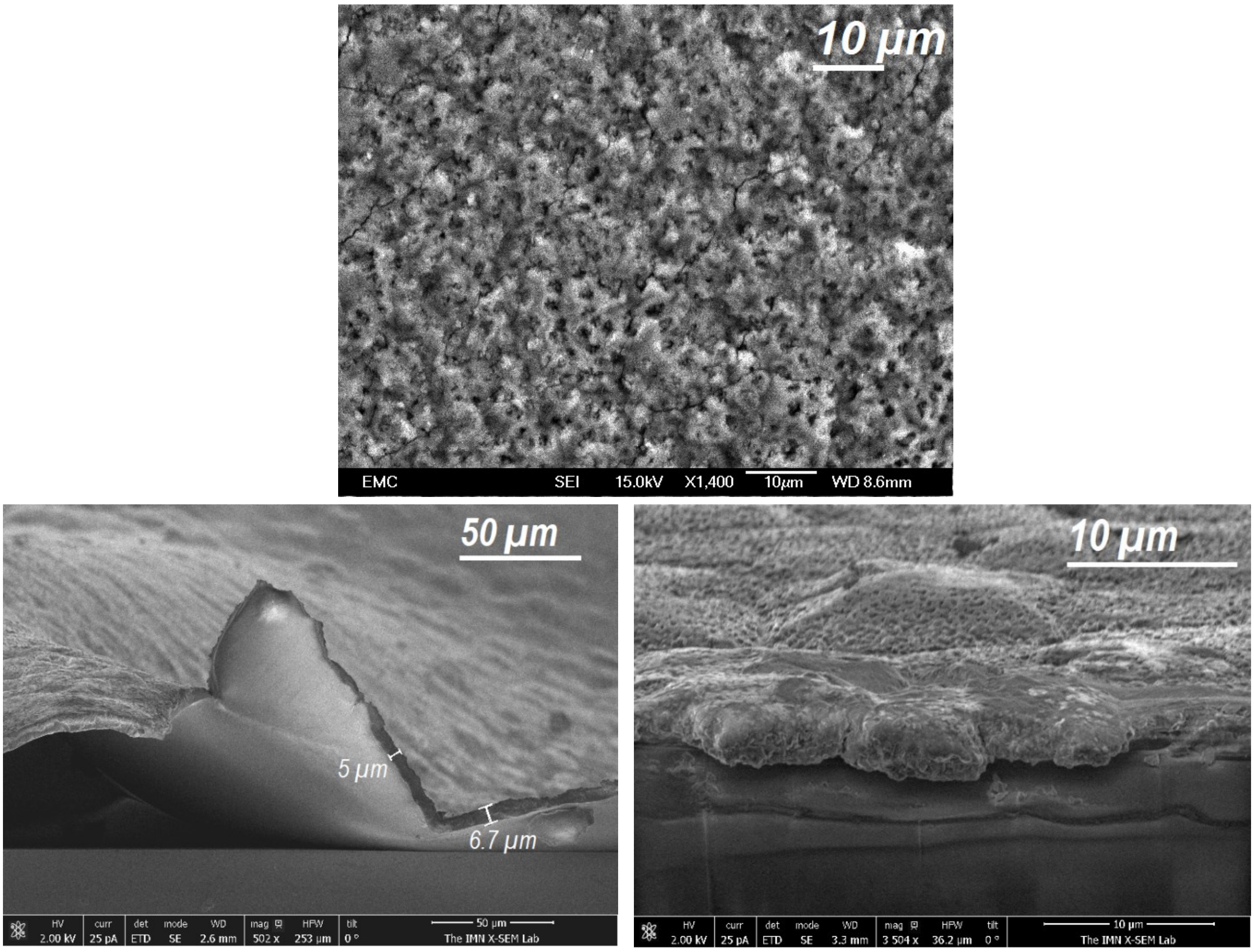

Figure S11. Seebeck coefficient determination of a 150 nm thick Cu film physically deposited onto glass. This was conducted as a control experiment only in order to compare the Seebeck coefficient values obtained for the $Cu_3(HHTP)_2$ thin films.

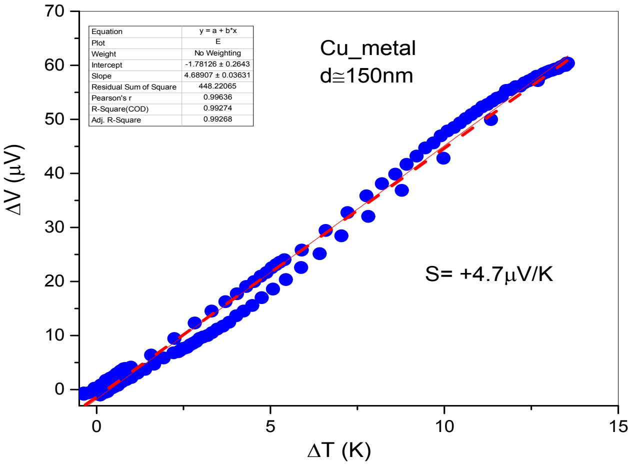

Equation	y = a + b*x
Plot	E
Weight	No Weighting
Intercept	-1.78126 ± 0.2643
Slope	4.68907 ± 0.03631
Residual Sum of Square	448.22065
Pearson's r	0.99636
R-Square(COD)	0.99274
Adj. R-Square	0.99268

Table S4. Summary of thermoelectric properties of Cu3(HTTP)2 pellet and thin film.

Metal-Organic Framework	**Synthesis method**	**Configuration**	***S* (µV/K)**	**σ (S/cm)**	**charge carrier concentration (cm^3)**	**Power factor (µW/m)**
$Cu_3(HHTP)_2$	Hydrothermal	bulk	-7.24	3.80 x10^{-3}	2.2 x10^{17}	2 x10^{-5}
$Cu_3(HHTP)_2$	Electrochemical	film	-121.4	2.28 x10^{-3}	4.97 x10^{16}	3.15 x10^{-3}

References

1. W. H. Li, K. Ding, H. R. Tian, M. S. Yao, B. Nath, W. H. Deng, Y. Wang and G. Xu, Adv. Funct. Mater., 2017, **27**, 1–7.
2. M. Hmadeh, Z. Lu, Z. Liu, F. Gándara, H. Furukawa, S. Wan, V. Augustyn, R. Chang, L. Liao, F. Zhou, E. Perre, V. Ozolins, K. Suenaga, X. Duan, B. Dunn, Y. Yamamto, O. Terasaki and O. M. Yaghi, Chem. Mater., 2012, **24**, 3511–3513.
3. L. Sun, M. G. Campbell and M. Dincə, Angew. Chemie - Int. Ed., 2016, 55, 3566–3579.
4. M. K. Smith, K. E. Jensen, P. A. Pivak and K. A. Mirica, Chem. Mater., 2016, **28**, 5264–5268.
5. M. S. Yao, X. J. Lv, Z. H. Fu, W. H. Li, W. H. Deng, G. D. Wu and G. Xu, Angew. Chemie - Int. Ed., 2017, **56**, 16510–16514.
6. Yao, M. S. et al. Layer-by-Layer Assembled Conductive Metal–Organic Framework Nanofilms for Room-Temperature Chemiresistive Sensing. Angew. Chemie - Int. Ed. **56**, 16510–16514 (2017).
7. V. Rubio-Giménez, M. Galbiati, J. Castells-Gil, N. Almora-Barrios, J. Navarro-Sánchez, G. Escorcia-Ariza, M. Mattera, T. Arnold, J. Rawle, S. Tatay, E. Coronado and C. Martí-Gastaldo, Adv. Mater., 2018, **30**, 1–8
8. B. Hoppe, K. D. J. Hindricks, D. P. Warwas, H. A. Schulze, A. Mohmeyer, T. J. Pinkvos, S. Zailskas, M. R. Krey, C. Belke, S. König, M. Fröba, R. J. Haug and P. Behrens, CrystEngComm, 2018, **20**, 6458–6471.
9. M. Ko, A. Aykanat, M. K. Smith and K. A. Mirica, Sensors, 2017, 17, 2192.
10. X. Song, X. Wang, Y. Li, C. Zheng, B. Zhang, C. Di, F. Li, C. Jin, W. Mi, L. Chen and W. Hu, Angew. Chemie Int. Ed., 2020, **59**, 1118−1123.
11. W. Zhou, S. Lv, X. Liu, Y. Li and J. Liu, Chem. Commun., 2019, **55**, 11207–11210.
12. L. Guo, J. Sun, W. Zhang, L. Hou, L. Liang, Y. Liu and C. Yuan, ChemSusChem, 2019, **12**, 5051–5058.
13. W. T. Koo, S. J. Kim, J. S. Jang, D. H. Kim and I. D. Kim, Adv. Sci., 2019, **6**, 1–10.
14. K. W. Nam, S. S. Park, R. dos Reis, V. P. Dravid, H. Kim, C. A. Mirkin and J. F. Stoddart, Nat. Commun., 2019, **10**, 1–10.
15. L. Guo, J. Sun, W. Zhang, L. Hou, L. Liang, Y. Liu and C. Yuan, ChemSusChem, 2019, **12**, 5051–5058.
16. A. Mahringer, A. C. Jakowetz, J. M. Rotter, B. J. Bohn, J. K. Stolarczyk, J. Feldmann, T. Bein and D. D. Medina, ACS Nano, 2019, **13**, 6711–6719.
17. K. J. Erickson, F. Léonard, V. Stavila, M. E. Foster, C. D. Spataru, R. E. Jones, B. M. Foley, P. E. Hopkins, M. D. Allendorf and A. A. Talin, Adv. Mater., 2015, **27**, 3453–3459.

18. X. Chen, Z. Wang, Z. M. Hassan, P. Lin, K. Zhang, H. Baumgart and E. Redel, ECS J. Solid State Sci. Technol., 2017, **6**, P150–P153.

19. L. Sun, B. Liao, D. Sheberla, D. Kraemer, J. Zhou, E. A. Stach, D. Zakharov, V. Stavila, A. A. Talin, Y. Ge, M. D. Allendorf, G. Chen, F. Léonard and M. Dincă, Joule, 2017, **1**, 168–177.

20. K. V. Selvan, M. N. Hasan and M. S. Mohamed Ali, J. Electron. Mater., 2019, **48**, 745–777.